International Journal of Heat and Mass Transfer 52 (2009) 4584–4591

Contents lists available at ScienceDirect

International Journal of Heat and Mass Transfer

journal homepage: www.elsevier.com/locate/ijhmt

Transient detailed numerical simulation of the combustion of carbon particles

R. Stauch *,[1], U. Maas

Institut für Technische Thermodynamik, Universität Karlsruhe (TH), Kaiserstrasse 12, D-76128 Karlsruhe, Germany

ARTICLE INFO

Article history:
Received 26 November 2007
Received in revised form 28 February 2008
Accepted 26 February 2009
Available online 11 May 2009

Keywords:
Carbon
Particle
Burning rate
Surface temperature

ABSTRACT

The burning process of a single carbon particle in air at isobaric conditions is studied. Transient numerical simulations, including detailed physical and chemical models, are performed. The characteristic values of the burning process, i.e., the burning rate and the surface temperature, show an unsteady behavior. However, if the particle radius is fixed artificially, a steady behavior of these values can be observed. Furthermore, it turns out that if the ambient temperature is sufficiently high, the d^2-law holds and the burning rate constant K (of the d^2-law) is almost constant in time. Thus, the burning process bears a strong resemblance to the transport controlled regime. These findings are confirmed by the obtained results of a minor dependence of the burning rate on the ambient pressure and an almost linear dependence of the burning rate on the oxygen concentration in the ambient gas phase.

1. Introduction

The ignition and combustion of a coal particle is a transient phenomenon with a spatial fine structure. The overall reaction process includes several aspects, like chemical kinetics on the surface, molecular transport of species and the chemical kinetics in the gas phase. The coupling of these different physical and chemical processes complicates the understanding of the behavior of coal particles. A suitable configuration to investigate the basic phenomena of these processes is given by the combustion of a single carbon particle in a quiescent gas environment. Because of the coupling a calculation of the combustion of carbon particles has to imply detailed models for the physical transport processes and for the chemical kinetics.

The ignition and combustion of coal particles have been studied experimentally [1–7] by many groups. Fewer numerical investigations have been reported [8,9]. Gururajan et al. [8], for example, presented a detailed model for the steady-state combustion of a coal particle under spherical symmetry. The temperature gradient within the particle as well as heat transfer by radiation is neglected. The Lewis number in the gas phase is assumed to be unity. Surface and gas phase kinetics are modeled by one-step kinetics. Mitchell et al. [9] studied the burning behavior of pulverized-coal char particles performing numerical quasi-steady-state calculations including a detailed gas phase reaction mechanism, a detailed surface reaction mechanism and a multicomponent transport formulation.

In order to focus on the heterogeneous combustion of carbon several authors have studied the combustion of graphite experimentally [10,11]. Makino et al. have determined combustion rates and global kinetic parameters of graphite in a stagnation flow [10,11]. Numerical simulations have been performed for the combustion of graphite [12] and carbon [13–18]. Libby and Blake studied the influence of water vapor on the burning process of carbon particles [13]. Frozen gas phase chemistry and equilibrium gas phase chemistry were used to simulate the burning process. Chelliah simulated the steady burning of spherical particles in a quiescent environment using detailed chemical and physical models [12]. A complex interaction between surface kinetics, gas phase kinetics, mass transport and thermal radiation was identified. Adomeit et al. simulated the combustion behavior of a carbon surface in a stagnation flow [14,15]. One step gas phase kinetics was used. It turned out that the interaction between physical and chemical processes, which determines the combustion rate, cannot be described in a reliable way by simply considering the limiting cases of frozen flow and infinitely fast homogeneous reaction [14]. Cho et al. presented a detailed model for the simulation of carbon particles [16]. Lee et al. [17] performed transient time-dependent simulations to investigate the influence of surface regression. They concluded that the assumption of quasi-steadiness is critical.

To improve the understanding of the coupling of the different physical and chemical processes the influence of different ambient conditions on characteristic quantities of the combustion of carbon particles, like surface temperature and burning rate, has to be investigated. In the following we study the influence of the time-dependence of the particle radius on the burning behavior. The

* Corresponding author. Tel.: +49 711 896 4538; fax: +49 711 8902 4538.
E-mail addresses: rainer.stauch@behrgroup.com (R. Stauch), maas@itt.mach.uni-karlsruhe.de (U. Maas).
[1] Present address: Behr GmbH & Co., KG, Siemensstraße 164, D-70469 Stuttgart, Germany.

0017-9310/$ - see front matter © 2009 Elsevier Ltd. All rights reserved.
doi:10.1016/j.ijheatmasstransfer.2009.02.047

Nomenclature

A_l	pre-exponential factor of reaction l (m, mol, s)
C_p	specific heat capacity at constant pressure (J/kg K)
D_i^m	diffusion coefficient of species i (m^2/s)
d	diameter (μm)
d_{part}	particle diameter (μm)
$E_{a,l}$	activation energy of reaction l (kJ/mol)
h_i	specific enthalpy (J/kg)
j_i	diffusion flux of species i (kg/m^2 s)
j_q	conductive heat flux density (W/m^2)
K	burning rate constant (m^2/s)
k_l	rate coefficient of reaction l (m, mol, s)
M_i	molar mass of species i (kg/mol)
$\overline{M}$	mean molar mass (kg/mol)
m_{part}	particle mass (kg)
p	pressure (bar)
R	universal gas constant (J/mol K)
R_i	surface reaction rate of species i (kg/m^2 s)
r	radial coordinate (m)
r_{part}	particle radius (μm)
T	temperature (K)
T_g	gas temperature (K)
T_{ref}	reference temperature (K)
T_{surf}	surface temperature (K)
t	time (s)
v_n	normal velocity (m/s)
w_i	mass fraction of species i
x_i	mole fraction of species i
z	mass flux at the surface of the particle (kg/s)

Greek symbols

β_l	temperature exponent of reaction l
ϵ	emissivity
λ	heat conductivity (W/m K)
ρ	density (kg/m^3)
σ	Stefan–Boltzmann constant ($W/m^2 K^4$)
ϕ	burning rate (kg/m^2 s)
ϕ_{stef}	Stefan flux (kg/m^2 s)
ψ	Lagrangian-like coordinate (kg)
$\dot{\omega}_i$	molar rate of formation of species i (mol/m^3)

Subscripts

i	species i
part	particle
0	initial value

Superscripts

g	gas phase
s	solid phase ($\triangleq$ particle)

usability of the assumption of no radiative loss is studied. Furthermore, the dependence of the burning rate and the surface temperature of properties of the ambient gas phase, like pressure, water concentration and oxygen concentration is investigated. For the simulations different surface mechanisms of Bradley et al. [19] and Libby and Blake [13] are used to model the surface kinetics. The results of the calculations, basing on different surface mechanisms are compared.

2. Numerical model

To investigate the interaction of the physical and chemical processes, detailed simulations are an efficient tool. Transient numerical simulations of the combustion of single carbon particles have been performed, starting with the deposition of the particle in an ambient gas phase, where both particle and gas phase have the same initial temperature.

2.1. Chemical and physical modeling

The particle represents nonporous graphite particle of 100% carbon with a density of 1800 kg/m^3. In the gas phase the chemical kinetics is based on a reaction mechanism of Maas and Warnatz [20] including 13 chemical species and 72 elementary reactions. The surface kinetics is based on the surface mechanism of Bradley et al. [19] and the surface mechanism of Libby and Blake [13], respectively. The surface mechanism of Bradley et al. consists of nine chemical species and five reactions. Libby and Blake propose a surface mechanism, including six chemical species and three reactions. The reactions of both mentioned surface mechanisms including the Arrhenius parameters are listed in Table 1. Rate coefficients of the surface reactions are expressed in the form

$$k_l = A_l T^{\beta_l} \exp\left(\frac{-E_{a,l}}{RT}\right), \quad (1)$$

Table 1
Reactions of the used surface mechanisms.

Reaction	$A_l/$(m, mol, s)	β_l	$E_{a,l}/$(kJ mol^{-1})
Surface mechanism of Bradley et al.			
$2C(so) + O_2 \rightarrow 2CO$	2.74×10^{-18}	6.5	63.64
$C(so) + CO_2 \rightarrow 2CO$	6.789×10^{7}	0.5	285.0
$C(so) + O \rightarrow CO$	4.548×10^{4}	0.5	0.0
$C(so) + H_2O \rightarrow H_2 + CO$	3.621×10^{9}	0.5	288.0
$C(so) + OH \rightarrow CO + H$	2.467×10^{4}	0.5	0.0
Surface mechanism of Libby and Blake			
$2C(so) + O_2 \rightarrow 2CO$	5.95×10^{2}	1.0	149.7
$C(so) + CO_2 \rightarrow 2CO$	1.687×10^{1}	1.0	175.1
$C(so) + H_2O \rightarrow H_2 + CO$	1.687×10^{1}	1.0	175.1

where the Arrhenius parameters A_l, β_l and $E_{a,l}$ denote the pre-exponential factor, the temperature exponent and the activation energy.

The ideal gas law is assumed to hold. The molecular transport processes in the gas phase are modeled in detail. The diffusion fluxes in the gas phase are calculated by the approximation of Curtiss and Hirschfelder [21–24] and the heat fluxes are modeled by Fouriers law [24–26]. The temperature dependence of the physical properties of the gas phase, like e.g., diffusion coefficients or heat conductivities, based on the kinetic theory of gases [22,24] are included in the used model. The carbon particle is assumed to have spherical shape during the complete combustion process. The heat loss by radiation at the surface of the particle is calculated following the Stefan–Boltzmann law [25,26]. The temperature dependence of the emissivity of carbon is taken from Siegel and Howell [27]. Heat conduction inside the carbon particle is regarded as well (see below for governing equation). Details of the modeling of the transport equations can be found in the mentioned literature [22–26] where the used equations are discussed.

2.2. Governing equations

Assuming a spherical symmetry the number of independent variables is reduced to two, namely the time t and the radial coordinate r.

$$\underbrace{f = f(x,y,z,t)}_{3D} \rightarrow \underbrace{f = f(r,t)}_{1D}. \tag{2}$$

To overcome numerical difficulties due to the discretization of the convective terms, the equation system is transformed into modified Lagrangian coordinates.

$$f(r,t) \rightarrow f(\psi,t), \tag{3}$$

$$\psi(r,t) = \int_{r_{part}}^{r} \rho(r,t) r^2 dr, \tag{4}$$

where r denotes the spatial coordinate, r_{part} the radius of the particle, t the time, ρ the density and ψ the Lagrangian-like coordinate. Due to the transformation the continuity equation is implicitly fulfilled. Instead of the continuity equation, the transformation equation is solved. Therefore, the governing equations in the gas phase read

$$\left(\frac{\partial r}{\partial \psi}\right)_t = \frac{1}{\rho r^2}, \tag{5}$$

$$\frac{\partial w_i}{\partial t} + z\frac{\partial w_i}{\partial \psi} + \frac{\partial}{\partial \psi}(r^2 j_i) = \frac{\dot{\omega}_i M_i}{\rho}, \tag{6}$$

$$\frac{\partial T}{\partial t} - \frac{1}{\rho C_p}\frac{\partial p}{\partial t} + z\frac{\partial T}{\partial \psi} - \frac{1}{C_p}\frac{\partial}{\partial \psi}\left(\rho r^4 \lambda \frac{\partial T}{\partial \psi}\right) - \frac{r^2}{C_p}\sum_{i=1}^{n_S} j_i C_{pi}\frac{\partial T}{\partial \psi} + \frac{1}{\rho C_p}\sum_{i=1}^{n_S}\dot{\omega}_i h_i M_i = 0, \tag{7}$$

$$\rho = \frac{p\overline{M}}{RT}, \tag{8}$$

where w_i is the mass fraction and j_i the diffusion flux of species i, $\dot{\omega}_i$ the molar rate of formation of species i, M_i the molar mass of species i, p the pressure, T the temperature, C_p the specific heat capacity at constant pressure, λ the heat conductivity, $\overline{M}$ the mean molar mass, R the universal gas constant, C_{pi} and h_i the specific heat capacity and the specific enthalpy of species i.

By introduction of the parameter z it is possible to fix the Lagrangian coordinate system at the surface of the particle. The value of z is given by

$$0 = \left(\frac{\partial r}{\partial t}\right)_\psi \bigg|_{\psi=\psi_0} = v(\psi_0) - \frac{z}{\rho(\psi_0) r_{part}^2}. \tag{9}$$

The ambient gas phase is assumed to be isobaric. Uniform pressure is assumed (low-Mach number approximation), and therefore the momentum conservation equation is replaced by [28]

$$\frac{\partial p}{\partial \psi} = 0. \tag{10}$$

For the solid phase only the energy equation has to be solved to account for the heat conduction inside the particle. The governing equation reads

$$\frac{\partial T}{\partial t} - \frac{\lambda^s}{\rho^s C_p^s}\cdot\frac{1}{r^2}\cdot\frac{\partial}{\partial r}\left(r^2\frac{\partial T}{\partial r}\right) = 0, \tag{11}$$

where λ^s is the heat conductivity of the particle, ρ^s the density of the particle and C_p^s the specific heat capacity of the particle.

2.3. Boundary conditions

Boundary conditions have to specified in the center of the particle as well as at the outer boundary. Additionally, interface equations have to be specified to account for the processes at the surface of the particle.

In the center of the particle the standard symmetry boundary condition is applied for the temperature. At the outer boundary, far away from the particle surface, Dirichlet boundary conditions are assumed for the ambient gas temperature and the species mass fractions of the ambient gas phase (see text and figures below for specific values).

The following interface equations describe the processes at the particle surface.

$$\phi_{stef} = \sum_i R_i, \tag{12}$$

$$0 = \rho^g \cdot v_n^g - \phi_{stef}, \tag{13}$$

$$0 = w_i^g \cdot \phi_{stef} - R_i + j_i^g, \tag{14}$$

$$0 = \phi_{stef}\cdot\left(\sum_i w_i^g h_i^g - h^s\right) + j_q^g + \sum_i h_i^g j_i^g - j_q^s - \epsilon\sigma(T^4 - T_{ref}^4). \tag{15}$$

The index g denotes the gas phase, the index s the solid phase. ϕ_{stef} denotes the Stefan flux, R_i the surface reaction rate of species i, ρ the density, v_n the velocity normal to the surface, w_i the mass fraction of species i, j_i the diffusion flux density of species i, j_q the conductive heat flux density, h_i the enthalpy of species i, ϵ the emissivity, σ the Stefan–Boltzmann constant and T_{ref} the reference temperature of the radiative heat loss which is set to 300 K.

The regression rate of the particle is given by

$$\frac{dr_{part}}{dt} = -\frac{\phi_{stef}}{\rho^s}, \tag{16}$$

where ρ^s denotes the density of the particle.

2.4. Numerical solution

The governing equations of the solid and the gas phase are solved in a fully coupled way. The differential-algebraic equation system is discretized by the method of lines using finite differences. The time integration is realized by the linearly implicit extrapolation method LIMEX. Details on the numerical solution can be found in [28,29,26].

3. Results and discussion

Numerical simulations are performed to investigate the influence of different ambient conditions on the burning behavior of carbon particles. The influence of the radiative loss at the particle surface on the burning behavior is studied. Furthermore, the dependence of the surface temperature and the burning rate of the particle on the ambient temperature, the ambient pressure and the mole fractions of water and oxygen is studied. Transient numerical simulations are performed starting with a thermalized carbon particle in a hot gas environment, i.e., both the particle and the gas phase have the same initial temperature which corresponds to the ambient gas temperature. These initial conditions are often not valid in real applications. However, the initial heat-up and ignition of the particle (from 0 to 1 s in Fig. 1) is not the scope of the study and, because the further combustion process is almost independent of the initial temperature it is of minor interest for the study. The surface kinetics is modeled by the reactions of Bradley et al. [19] and Libby and Blake [13]. The results of the mechanism of Bradley et al. are denoted by MECH1 in the following. The results of the calculations using the mechanism of Libby and Blake are denoted by MECH2.

3.1. Influence of the particle radius

Several published numerical studies of the combustion of particles consisting of carbon or coal assume a quasi-steady burning of the particle [13,8,9,12]. Following this assumption the particle

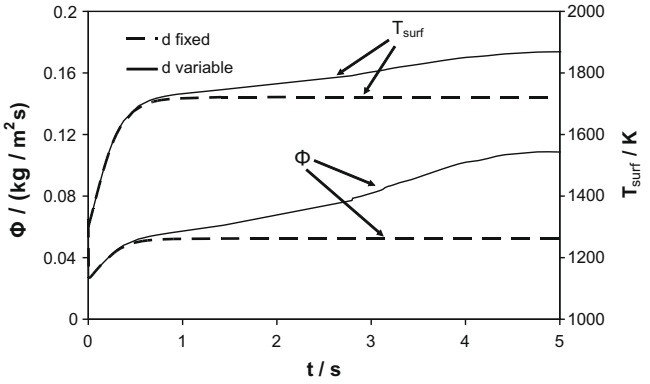

Fig. 1. Evolution of surface temperature and burning rate with time ($p = 1.01$ bar, $r_{part}(0) = 250$ μm,2% H_2O).

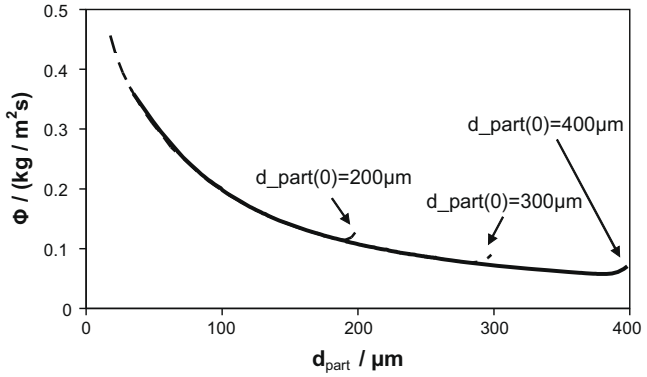

Fig. 2. Dependence of the burning rate on the particle diameter for three different initial diameters ($p = 1.01$ bar,$T_g = 1650$ K,12% O_2, 72% N_2, 16% H_2O).

radius does not vary with time during the combustion process. Rather, the particle radius is fixed to a certain value during one simulation of the combustion process. Note, that a parametric variation of the particle radius can be performed by several simulations. However, such calculations do not account for the dynamic particle consumption during the combustion process. The decrease of the particle radius causes a transient behavior of the particle during the combustion process. Characteristic values of the combustion process, like surface temperature and mass burning rate, depend on the particle radius [12]. Due to the time-dependence of the particle radius, these values vary with time during the combustion process. Lee et al. have shown the assumption of the steadiness of the particle radius to be critical [17].

To investigate the influence of the assumption of quasi-steady burning of carbon particles simulations are performed where the particle radius is fixed artificially (which is analogous to the above mentioned steadiness of the particle radius). This is done by omitting Eq. (16) during the numerical solution procedure. The results of these calculations are compared with results of calculations using the complete numerical model presented above where the particle radius of the particle decreases with time. If the particle radius is fixed artificially in numerical simulations a time evolution into a steady-state behavior can be observed. In Fig. 1, a representative time evolution of the burning rate ϕ and the surface temperature with variable (time-dependent) and fixed particle radius can be seen. The mentioned unsteadiness is not associated with the initial heating up and ignition of the particle (from 0 to 1 s in Fig. 1), where a unsteady behavior can be observed in both cases. In fact, a transient behavior of the surface temperature and the burning rate is obtained during the whole simulation time, if the particle radius is not fixed artificially. In the case of the fixed particle radius, a steady behavior is obtained after 0.5 s. In the case of the decreasing particle diameter a steady behavior cannot be observed until the particle has disappeared. In the following, the dependence of the characteristic quantities of the burning process, burning rate and surface temperature, is studied in more detail. Figs. 2 and 3 show the dependences of the burning rate and the surface temperature on the particle diameter for three simulations with different initial diameters ($d_{part}(0) = 200$ μm, $d_{part}(0) = 300$ μm,$d_{part}(0) = 400$ μm) and identical other ambient conditions. It should be noted that the time evolution of the depicted trajectories emerges from right to left in the figures starting at the initial value of the diameter which subsequently decreases. The three trajectories of the simulations in Fig. 2 approach the same curve after a short transient period. This curve seems to fit to a hyperbolic shape. The behavior of approaching the same curve can be observed for both the burning rate and the surface temperature. The surface temperature during the combustion process is lower than the initial temperature of 1650 K (see Fig. 3). The surface temperature is governed by the thermal equilibrium at the particle surface, which is dominated by the thermal radiation in the studied case. This is the reason, why the surface temperature of the particle is lower than the temperature of the ambient gas phase.

It can be stated that the characteristic values of the burning process are only dependent on the current particle diameter, independent of its previous evolution (note that the current diameter is different from the initial diameter). This holds, even though the characteristic values and the particle diameter are time-dependent. The graph of the dependence of the burning rate on the particle diameter shows a hyperbolic shape, if the burning rate ϕ is proportional to the inverse of the particle radius: $\phi \sim 1/r$. This shows the analogy to droplet evaporation. In the case of a steadily evaporating liquid droplet the d^2-law

$$d^2 = d_0^2 - Kt \tag{17}$$

describes the time evolution of the droplet diameter d [30,17,24]. Here, d_0 represents the initial diameter and K is the burning rate constant, which is time-independent. If the d^2-law is valid, the burning rate ϕ reads as

$$\phi = \frac{1}{4\pi r_{part}^2} \cdot \frac{dm_{part}}{dt} = \frac{\rho^s}{8} \cdot \frac{K}{r_{part}}. \tag{18}$$

Here, ρ^s is the density of the particle, which is assumed to be constant in the simulation, r_{part} is the particle radius and the burning rate constant K is the factor of proportionality in the d^2-law. In Fig. 4, the obtained time evolution of the particle diameter can be seen, which is in accordance with the previously obtained results.

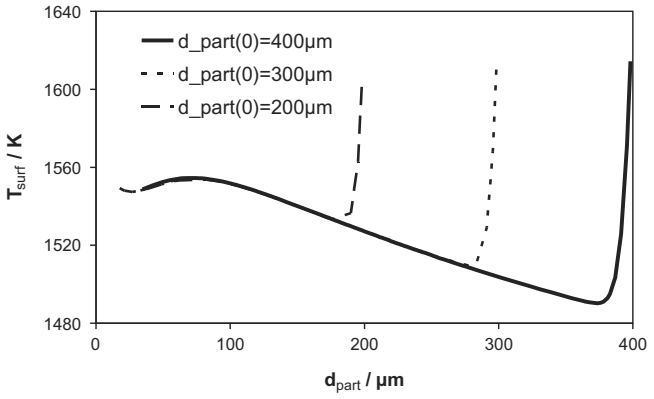

Fig. 3. Dependence of the surface temperature on the particle diameter for three different initial diameters ($p = 1.01$ bar,$T_g = 1650$ K,12% O_2, 72% N_2, 16% H_2O).

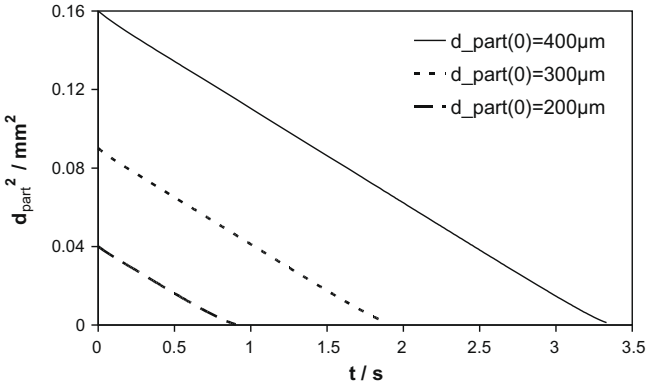

Fig. 4. Evolution of the particle diameter with time ($p = 1.01$ bar, $T_g = 1650$ K, 12% O_2, 72% N_2, 16% H_2O).

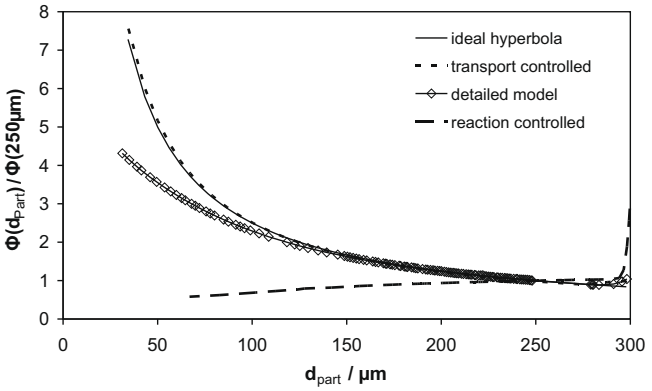

Fig. 5. Comparison of dependence of burning rate on the particle diameter in the transport controlled and the reaction controlled case ($p = 1.01$ bar, $T_g = 1650$ K, 12% O_2, 72% N_2, 16% H_2O).

The validity of these relations can be explained by the fact that the burning process of the carbon particle proceeds in the transport controlled regime [14]. The validity of this conclusion shall now be investigated in more detail. In Fig. 5, the dependence of the normalized burning rate on the particle diameter is shown for four different cases. In the transport controlled regime $K = \text{const.}$ holds [30,17,24] and the dependence of the burning on the particle diameter is given by the ideal hyperbolic curve

$$\phi = \frac{\rho^s}{4} \cdot \frac{K}{d_{part}}, \quad K = \text{const.} \rightarrow \frac{\phi(d_{part})}{\phi(d_{part} = 250\ \mu\text{m})} = \frac{250\ \mu\text{m}}{d_{part}}, \tag{19}$$

as in the case of a steadily evaporating liquid droplet, which is also a transport controlled process [30,24]. To mimic the transport controlled limit the surface kinetics is artificially accelerated by a multiplication of the reaction rates by a factor of 10^3. As can be seen, the curves of the accelerated kinetics (transport controlled) and the transport controlled limit (ideal hyperbola) coincide. To mimic the reaction controlled case the surface kinetics is artificially decelerated by multiplying the surface reaction rates by a factor of 10^{-3}. As can be seen in Fig. 5 the dependence of the burning rate on the particle diameter is minor in this case (reaction controlled). Additionally, the diameter dependence of the burning rate is shown in Fig. 5 in the case of the detailed model. In this case (detailed model) the shape of the curve resembles much more the transport controlled limit than the reaction controlled limit. These findings are confirmed by Fig. 6, in which the spatial profiles of oxygen

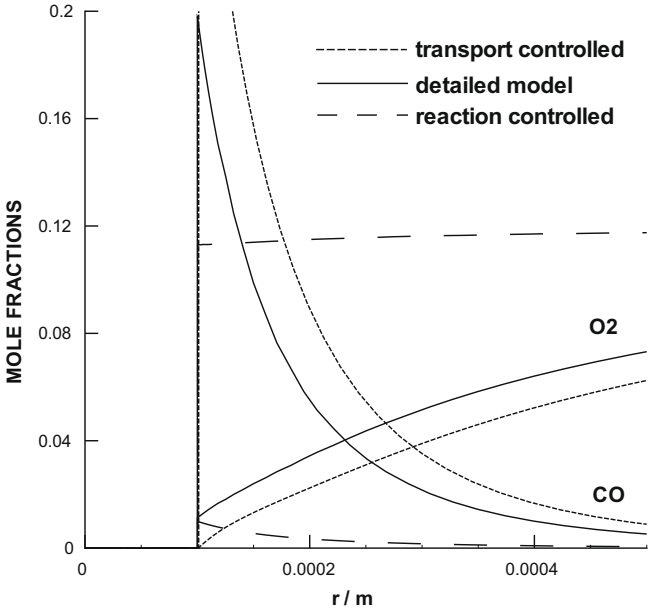

Fig. 6. Comparison of the spatial profiles in the boundary layer in the transport controlled and the reaction controlled case ($r_{part} = 100$ µm, $p = 1.01$ bar, $T_g = 1650$ K, 12% O_2, 72% N_2, 16% H_2O).

and carbon monoxide in the boundary layer of the particle are shown. Again, it can be seen that the profile of the studied case using the detailed model resembles more the profile of the transport controlled case than the profile of the reaction controlled case.

The presented data has been calculated with the use of MECH1. Nevertheless, the mentioned conclusions also hold for the use of MECH2 as well as for the other studied ambient conditions, if the ambient gas temperature is sufficiently high. The comparison of the dependence of the burning rate of MECH1 and MECH2 to the numerical data of Chelliah [12] and Mitchell et al. [9] is illustrated in Fig. 7. The qualitative behavior of the increase of the burning rate with decreasing particle diameter is the same for all datasets. Nevertheless, quantitative differences in the results cannot be ignored. The burning rate of both studied mechanisms exceed the burning rates taken from literature, whereas the shape of the curve of MECH1 bears more resemblance to the curve of Chelliah, than the curve of MECH2 does. On the other hand the burning rates of MECH2 almost coincide with the burning rates of Chelliah for particle diameter greater than 100 µm. The burning rates of all other

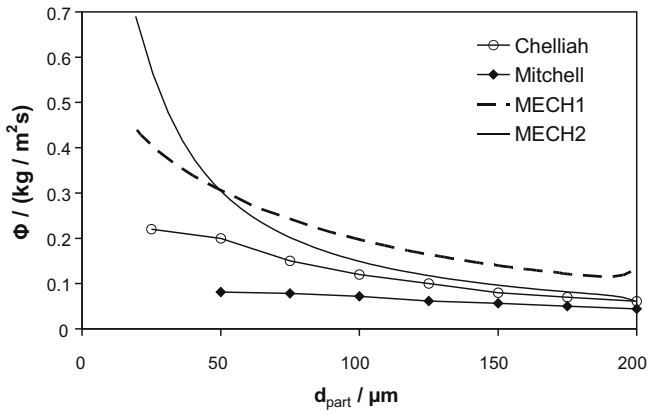

Fig. 7. Comparison of variations of the burning rate with particle diameter ($p = 1.01$ bar, $T_g = 1650$ K, 12% O_2, 72% N_2, 16% H_2O).

datasets are larger than the burning rates of Mitchell et al. for all diameters. It has to be noted that the mechanism of Mitchell et al. has been developed for simulations of the quasi-steady burning of coal char particles, which differ from the unsteady calculations of carbon particles performed here. Generally, the burning rates differ most for smaller particle diameters. The differences can be attributed, at least partially, to numerical inaccuracies. A decrease of the burning rate with decreasing particle diameter has been observed, if the grid resolution next to the particle surface is insufficient. Therefore, our simulations are performed on a grid with a high resolution in the boundary layer. Due to the different length scales of combustion processes, a regridding procedure based on a grid function is implemented [22,28,23]. Hence, the ratio of the distances of two neighboring grid points is adaptive. A representative distance in the boundary layer is 2 μm. During the performed simulations a decrease in the burning rates for small particle diameters has been observed in the case of coarser grids in the boundary layer. Besides that, the burning rates of the studied cases differ because of different reaction rates of the specific mechanisms.

Because of the above mentioned unsteadiness of the results of the transient simulations with variable particle radius, the characteristic values of the combustion process also vary during the simulation in contrast to steady-state calculations where each of these quantities takes one certain value. Therefore, the characteristic values of the combustion process are determined at a certain radius in the following to compare with the results of steady-state calculations.

3.2. Influence of radiative loss

In Fig. 8, the variation of the surface temperature with the ambient gas temperature is shown for the surface reaction mechanism of Bradley et al. (MECH1) and Libby and Blake (MECH2). The open symbols represent the obtained results under the assumption of no radiative loss of the surface of the particle. As one can see the results are in good agreement with the results of Chelliah [12], who has also assumed negligible thermal radiation. In contrast, the filled symbols depict the surface temperatures including heat loss due to radiation at the surface of the particle. The surface temperature in this case shows a similar ambient temperature dependence as in the case of no radiation. However, the absolute surface temperature is about 600 K lower. The surface temperatures of both mechanisms show a slightly larger slope in the case of no radiation than in the case of radiation. In both cases the curves of MECH1 display larger slopes than the curves of MECH2. MECH1 appears to be more sensitive on the variation of the ambient temperature than MECH2. So it can be stated that the inclusion of radiative loss at the particle surface has a significant influence on the surface temperature in the case of the combustion of a single carbon particle. According to this surface temperature the reaction rates and in conclusion the burning rates vary. Certainly, if the particle is surrounded by other particles, like in a pulverized coal flame, the overestimation of the surface temperature is less than in the case of a single particle. However, the decrease of this overestimation is dependent on the concentration of the particles. Due to the results in this section the radiation loss at the surface is included in the following calculations.

3.3. Influence of ambient pressure

To determine the sensitivity of the burning rate with respect to the ambient pressure and to verify the above mentioned conclusions of the transport controlled burning process the influence of the ambient pressure on the burning process is investigated. Fig. 9 shows the dependence of the burning rate and the surface temperature on the ambient pressure in the range from 0.5 to 25 bar. Both the burning rate and the surface temperature show almost no dependence on the ambient pressure. Only for pressures $\leqslant 5$ bar a slight increase of the burning rate with increasing pressure can be observed. This behavior is not affected by the ambient temperature, if the temperature is sufficiently high. The obtained results comply with Croiset et al. [7] who stated a minor variation of the burning rate with pressure. If the burning process is transport controlled, the burning rate is proportional to the gas phase mass diffusion flux at the surface. Following the approximation of Curtiss and Hirschfelder, it holds for the mass diffusion flux $j_{m,i}$ [21,25,24]

$$j_{m,i} = -D_i^m \rho \frac{w_i}{x_i}\frac{\partial x_i}{\partial r} = -D_i^m \rho \frac{M_i}{\overline{M}}\frac{\partial x_i}{\partial r}, \quad D_i^m(p) \sim \frac{1}{p} \Rightarrow j_{m,i} \neq f(p), \tag{20}$$

where D_i^m represents the diffusion coefficient, w_i the mass fraction, x_i the mole fraction and M_i the molar mass of species i, ρ the density, $\overline{M}$ the mean molar mass, p the pressure and r the spatial coordinate. Eq. (20) shows the independence of the mass diffusion flux on the pressure. Therefore, the independence of the burning rate (cf. Fig. 9) on the pressure corresponds with the independence of the mass diffusion flux on the pressure. On the other hand, the surface reaction rates are not independent of the ambient pressure due to its dependence on the concentrations of the involved species of the gas phase. Hence, if the burning process is reaction controlled, the burning rate would not be independent of the pressure. There-

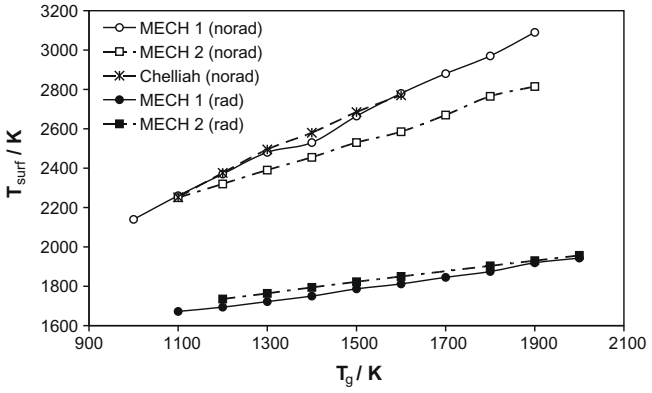

Fig. 8. The variation of the surface temperature with ambient gas temperature with and without radiation loss at the particle surface ($p = 1.01$ bar, $d_{part}(0) = 400$ μm, 1% H_2O).

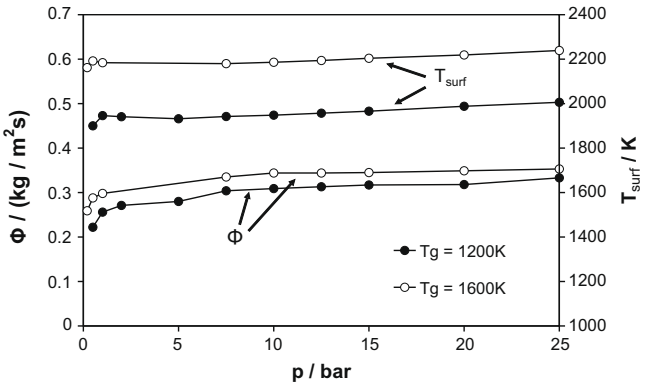

Fig. 9. The variation of the burning rate and surface temperature with ambient pressure ($d_{part} = 100$ μm, 2% H_2O).

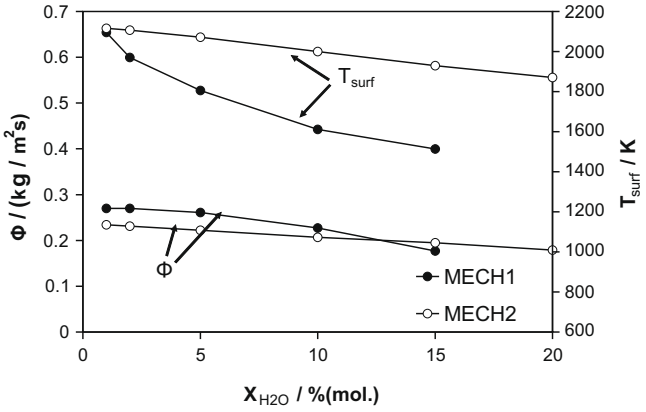

Fig. 10. The variation of the burning rate and surface temperature with the concentration of water in air ($p = 1.01$ bar, $d_{part} = 100$ μm, $T_g = 1200$ K).

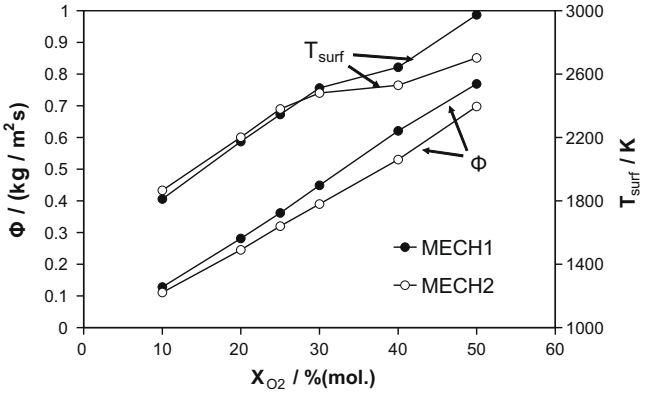

Fig. 11. The variation of the burning rate and surface temperature with the concentration of oxygen in the ambient gas phase ($p = 1.01$ bar, $d_{part} = 100$ μm, $T_g = 1600$ K, 2% H_2O).

fore, the independence of the burning on the pressure confirms the conclusion that the burning process proceeds in the transport controlled regime.

3.4. Influence of water concentration

In the case of the burning of a carbon particle the presence of gaseous water is of crucial importance for the gas phase kinetics [31,20,24]. In the following the influence of the ambient gas composition on the burning behavior is investigated. The dependence of the burning rate and the surface temperature on the mole fraction of water in the range from 1% to 20% is shown in Fig. 10 for the two surface reaction mechanisms MECH1 and MECH2. For both mechanisms both the burning rate and the surface temperature decrease with increasing mole fraction of water in the gas phase. Nevertheless, the steeper decrease of both values in the case of MECH1 should be noticed. In the case of the surface temperature the obtained difference is significant, whereas the differences of the burning rates are within a range of 20%. So it can be stated that the mechanism of Bradley et al. (MECH1) shows a considerably larger sensitivity to the variation of the mole fraction of water in the gas phase than the mechanism of Libby and Blake (MECH2).

3.5. Influence of oxygen concentration

If the burning process is transport controlled by the diffusion flux of oxygen, a variation of the oxygen concentration of the ambient gas phase has to lead to a noticeable change in the burning rate of the particle. Fig. 11 shows the dependence of the burning rate and the surface temperature on the mole fraction of oxygen of the ambient gas phase. Again, for both surface mechanisms (MECH1, MECH2) comparable results are obtained. The differences of the burning rate and the surface temperature are within a range of 20%, whereas the qualitative behaviors of both mechanisms coincide. The surface temperature appears to have a linear dependence on the oxygen concentration up to a mole fraction of oxygen of 30% with a noticeable bend of the curve at about 2600 K due to the increasing decomposition of molecular hydrogen with increasing temperature. The molecular hydrogen originates from the particle surface by the corresponding surface reaction (cf. Table 1). The linear dependence of the burning rate holds for the complete range of the oxygen mole fraction from 10% to 50%. Because the mass diffusion flux in the gas phase also shows a linear dependence on the spatial gradient of the oxygen concentration (cf. Eq. (20), [25]), a strong dependence of the burning rate on the diffusion flux of oxygen in the gas phase arises. The obtained results lead to the conclusion that mainly the oxygen diffusion flux is the rate limiting transport process of the burning process for the studied conditions of ambient gas temperatures $\geqslant 1100$ K and ambient pressures $\geqslant 1$ bar.

4. Conclusions

Transient numerical simulations of the burning process of a carbon particle in air including detailed physical and chemical models have been performed. A temporarily steady behavior cannot be observed, because of the time-dependent particle radius. If the radius is fixed artificially during the simulations, a steady-state behavior is obtained. However, after a short transient period the dependences of the characteristic values of the burning behavior, like burning rate or surface temperature, on the particle diameter are identical, even if simulations are performed with different initial particle radii. The burning rate constant K, which represents the factor of proportionality in the d^2-law is found to be almost constant in time, even if the particle radius is not fixed artificially. These findings lead to the conclusion that for sufficiently high ambient temperatures and ambient pressures the burning process is transport controlled, which is confirmed by the studies of the dependence of the burning rate and the surface temperature on the ambient pressure as well as on the composition of the ambient gas phase. The findings are in accordance with the conclusion of Nettleton and Stirling [32].

Furthermore, it is ascertained that neglecting the heat loss at the particle surface leads to an overestimation of the surface temperature of about 600 K in the case of single carbon particles. Almost no dependence of the surface temperature and the burning rate on the ambient pressure is obtained. In contrast, the burning rate is found to increase almost linearly with the oxygen concentration of the ambient gas phase. Additionally, a decrease of the burning rate with increasing water concentration of the gas phase is observed. Hence, the oxygen diffusion flux is supposed to be the rate limiting factor.

Qualitatively equal results are obtained using the surface reaction mechanism of Libby and Blake instead of the mechanism of Bradley et al. In some extent this consistency can be attributed to the fact that the burning process is mainly transport-controlled. However, significant quantitative differences occur, especially in the case of the surface temperature, where the mechanism of Bradley et al. shows a higher sensitivity of the surface temperature on the variation of ambient conditions.

Acknowledgements

The authors thank the DFG for financial support in the frame of SFB 606 and of the project "Reduzierte kinetische Modelle für die

Abscheidung von Kohlenstoff aus der Gasphase" of the DFG-Paketantrag "Pyrolytischer Kohlenstoff aus der Gasphase – von der Elementarreaktion zur Prozess-Simulation".

References

[1] I. Smith, The kinetics of combustion of pulverized semi-anthracite in the temperature range 1400–2200 K, Combust. Flame 17 (1971) 421–428.
[2] W. Seeker, W. Lester, J. Merklin, Shock tube techniques in the study of pulverized coal ignition and burnout, Rev. Sci. Instrum. 51 (11) (1980) 1523–1531.
[3] B. Young, I. Smith, The kinetics of combustion of petroleum coke particles at 1000 to 1800 K: the reaction order, Proc. Combust. Inst. 18 (1981) 1249–1255.
[4] P. Brooks, R. Essenhigh, Variation of ignition temperatures of fuel particles in vitiated oxygen atmospheres: determination of reaction mechanism, Proc. Combust. Inst. 21 (1986) 293–302.
[5] W. Rybak, M. Zembrzuski, I. Smith, Kinetics of combustion of petroleum coke and sub-bituminous coal char: results of ignition and steady-state techniques, Proc. Combust. Inst. 21 (1986) 231–237.
[6] V. Cozzani, L. Petarca, S. Pintus, L. Tognotti, Ignition and combustion of single, levitated char particles, Combust. Flame 103 (1995) 181–193.
[7] E. Croiset, C. Mallet, J.-P. Rouan, J.-R. Richard, The influence of pressure on char combustion kinetics, Proc. Combust. Inst. 26 (1996) 3095–3102.
[8] V. Gururajan, T. Wall, R. Gupta, J. Truelove, Mechanisms for the ignition of pulverized coal particles, Combust. Flame 81 (1990) 119–132.
[9] R. Mitchell, R. Kee, P. Glarborg, M. Coltrin, The effect of co-conversion in the boundary layers surrounding pulverized-coal char particles, Proc. Combust. Inst. 23 (1990) 1169–1176.
[10] A. Makino, N. Araki, Y. Mihara, Combustion of artificial graphite in stagnation flow: estimation of global kinetic parameters from experimental results, Combust. Flame 96 (1994) 261–274.
[11] A. Makino, T. Namikiri, K. Kimura, Combustion rates of graphite rods in the forward stagnation field with high-temperature airflow, Combust. Flame 132 (2003) 743–753.
[12] H. Chelliah, The influence of heterogeneous kinetics and thermal radiation on the oxidation of graphite particles, Combust. Flame 104 (1996) 81–94.
[13] P. Libby, T. Blake, Burning carbon particles in the presence of water vapor, Combust. Flame 41 (1981) 123–147.
[14] G. Adomeit, W. Hocks, K. Hendriksen, Combustion of a carbon surface in a stagnation point flow field, Combust. Flame 59 (1985) 273–288.
[15] K. Henricksen, W. Hooks, G. Adomeit, Combustion of a carbon surface in a stagnation point flow field – Part ii: Ignition and quench phenomena, Combust. Flame 71 (1988) 169–177.
[16] S. Cho, R. Yetter, F. Dryer, A computer model for one-dimensional mass and energy transport in and around chemically reacting particles, including complex gas-phase chemistry, multi-component molecular diffusion, surface evaporation, and heterogeneous reaction, J. Comput. Phys. 102 (1992) 160–179.
[17] J. Lee, R. Yetter, F. Dryer, Transient numerical modeling of carbon particle ignition and oxidation, Combust. Flame 101 (1995) 387–398.
[18] J. Lee, A. Tomboulides, S. Orszag, R. Yetter, F. Dryer, A transient two-dimensional chemically reactive flow model: fuel particle combustion in a nonquiescent environment, Proc. Combust. Inst. 26 (1996) 3059–3065.
[19] D. Bradley, G. Dixon-Lewis, S. El-DinHabik, E. Mushi, The oxidation of graphite powder in flame reaction zones, Proc. Combust. Inst. 20 (1984) 931–940.
[20] U. Maas, J. Warnatz, Ignition processes in carbon monoxide–hydrogen–oxygen mixtures, Proc. Combust. Inst. 22 (1988) 1695–1704.
[21] J. Hirschfelder, C. Curtiss, R. Bird, Molecular Theory of Gases and Liquids, John Wiley & Sons, New York, 1964.
[22] U. Maas, Mathematische Modellierung instationärer Verbrennungsprozesse unter Verwendung detaillierter chemischer Reaktionsmechanismen, Ph.D. thesis, Universität Heidelberg, 1988.
[23] U. Maas, J. Warnatz, Simulation of chemically reacting flows in two-dimensional geometries, Impact Comput. Sci. Eng. 1 (1989) 394–420.
[24] J. Warnatz, U. Maas, R. Dibble, Combustion, third ed., Springer, Berlin, 2001.
[25] R. Bird, W. Steward, E. Lightfoot, Transport Phenomena, John Wiley & Sons, New York, Chichester, Brisbane, Toronto, Singapore, 1960.
[26] R. Stauch, Detaillierte Simulation von Verbrennungsprozessen in Mehrphasensystemen, Ph.D. thesis, Universität Karlsruhe (TH), 2007.
[27] R. Siegel, J. Howell, Thermal Radiation Heat Transfer, second ed., McGraw-Hill, 1981.
[28] U. Maas, J. Warnatz, Ignition processes in hydrogen–oxygen mixtures, Combust. Flame 74 (1988) 53–69.
[29] R. Stauch, S. Lipp, U. Maas, Detailed numerical simulations of the auto-ignition of single *n*-heptane droplets in air, Combust. Flame 145 (2006) 533–542.
[30] C. Law, Recent advances in droplet vaporization and combustion, Prog. Energy Combust. Sci. 8 (1982) 171–201.
[31] F. Skinner, L. Smoot, Heterogeneous reactions of char and carbon, in: L. Smoot, D. Pratt (Eds.), Pulverized-Coal Combustion and Gasification, Plenum Press, New York, 1979, pp. 149–167.
[32] M. Nettleton, R. Stirling, The combustion of clouds of coal particles in shock-heated mixtures of oxygen and nitrogen, Proc. R. Soc. Lond. A Math. Phys. Eng. Sci. 322 (1971) 207–221.